Monthly Notices
of the
ROYAL ASTRONOMICAL SOCIETY

MNRAS **455,** 308–317 (2015) doi:10.1093/mnras/stv2250

Dark matter and IMF normalization in Virgo dwarf early-type galaxies

C. Tortora,* F. La Barbera and N. R. Napolitano

INAF – Osservatorio Astronomico di Capodimonte, Salita Moiariello, 16, I-80131 Napoli, Italy

Accepted 2015 September 27. Received 2015 September 27; in original form 2015 April 29

ABSTRACT

In this work, we analyse the dark matter (DM) fraction, $f_{\rm DM}$, and mass-to-light ratio mismatch parameter, $\delta_{\rm IMF}$ (computed with respect to a Milky Way-like initial mass function), for a sample of 39 dwarf early-type galaxies in the Virgo cluster. Both $f_{\rm DM}$ and $\delta_{\rm IMF}$ are estimated within the central (one effective radius) galaxy regions, with a Jeans dynamical analysis that relies on galaxy velocity dispersions, structural parameters, and stellar mass-to-light ratios from the SMAKCED survey. In this first attempt to constrain, simultaneously, the initial mass function (IMF) normalization and the DM content, we explore the impact of different assumptions on the DM model profile. On average, for an Navarro, Frenk & White (NFW) profile, the $\delta_{\rm IMF}$ is consistent with a Chabrier-like normalization ($\delta_{\rm IMF} \sim 1$), with $f_{\rm DM} \sim 0.35$. One of the main results of this work is that for at least a few systems the $\delta_{\rm IMF}$ are heavier than the Milky Way-like value (i.e. either top- or bottom-heavy). When introducing tangential anisotropy, larger $\delta_{\rm IMF}$ and smaller $f_{\rm DM}$ are derived. Adopting a steeper concentration–mass relation than that from simulations, we find lower $\delta_{\rm IMF}$ ($\lesssim 1$) and larger $f_{\rm DM}$. A constant M/L profile with null $f_{\rm DM}$ gives the heaviest $\delta_{\rm IMF}$ ($\sim$2). In the MONDian framework, we find consistent results to those for our reference NFW model. If confirmed, the large scatter of $\delta_{\rm IMF}$ for dEs would provide (further) evidence for a non-universal IMF in early-type systems. On average, our reference $f_{\rm DM}$ estimates are consistent with those found for low-$\sigma_{\rm e}$ ($\sim 100\,{\rm kms}^{-1}$) early-type galaxies (ETGs). Furthermore, we find $f_{\rm DM}$ consistent with values from the SMAKCED survey, and find a double-value behaviour of $f_{\rm DM}$ with stellar mass, which mirrors the trend of dynamical M/L and global star formation efficiency (from abundance matching estimates) with mass.

Key words: galaxies: dwarf – galaxies: elliptical and lenticular, cD – galaxies: evolution – galaxies: general – galaxies: kinematics and dynamics – galaxies: stellar content.

1 INTRODUCTION

Dark matter (DM) is a ubiquitous component of the universe and dominates the mass density of virialized objects as galaxies and clusters of galaxies. The current scenario of galaxy evolution predicts that structures form bottom–up, i.e. the smallest haloes form first, and then, larger and more massive haloes are created from the merging of such smaller objects. Within this scenario, numerical simulations of (DM only) structure formation within the standard Λ cold dark matter (ΛCDM) framework have provided accurate predictions on the DM density distribution from dwarf to massive galaxies, up to bigger structures, such as clusters of galaxies (Navarro, Frenk & White 1996; Bullock et al. 2001; Macciò, Dutton & van den Bosch 2008). However, more realistic models have been produced to evaluate the effect of baryons on the DM distribution (e.g. Gnedin et al. 2004).

No model of galaxy formation can be complete without an understanding of how dwarf galaxies form, as these systems are the closest objects, in the nearby Universe, to the building blocks of present, more massive, galaxies. Their shallow potential wells make them susceptible to a large variety of processes, from supernova feedback, to externally induced effects, such as photoionization and heating from cosmic UV background, as well as environmental processes, such as tidal interactions and ram-pressure stripping (Dekel & Birnboim 2006; Recchi 2014). This makes dwarf galaxies challenging to model, but at the same time, excellent laboratories to test important ingredients of astrophysics.

Providing a picture of the formation and evolution of dwarf galaxies implies to understand the origin of their luminous and dark mass components. In this regard, together with age and metallicity, the stellar initial mass function (IMF) is a key stellar ingredient, as varying the IMF can lead to variations of a factor of $\sim$2 into the mass scale of galaxies. Direct counts in the Milky Way (MW) have originally characterized the IMF as a power-law mass distribution, $dN/dM \propto M^{-\alpha}$, with $\alpha \sim 2.35$ (Salpeter 1955), and subsequently refined it to flatten at lower masses ($M \lesssim 0.5\,{\rm M}_{\odot}$; Kroupa 2001; Chabrier 2003). The IMF has been initially considered as universal across galaxy types and cosmic time, mostly because of a lack of evidence of IMF variations among stellar clusters and OB associations

*E-mail: ctortora@na.astro.it

in our Galaxy. This assumption has been recently questioned by a loud chorus of dynamical, lensing, and stellar population studies, finding evidence for systematic IMF variations in massive early-type galaxies (ETGs; Treu et al. 2010; Thomas et al. 2011; Conroy & van Dokkum 2012; Cappellari et al. 2012, 2013; Spiniello et al. 2012; Wegner et al. 2012; Dutton et al. 2013; Ferreras et al. 2013; Goudfrooij & Kruijssen 2013; La Barbera et al. 2013; Tortora, Romanowsky & Napolitano 2013; Weidner et al. 2013; Goudfrooij & Kruijssen 2014; Shu et al. 2015; Tortora et al. 2014b,a). These independent lines of evidence are interpreted with an excess of low-mass stars in high- (relative to low-)mass ETGs, implying lower DM fractions in these systems than found under the assumption of a universal, MW-like, distribution (e.g. Cappellari et al. 2013; Tortora et al. 2013). However, evidence for a heavier IMF normalization, than the MW-like one, has been recently questioned for three nearby massive galaxies by Smith (2014) and Smith, Lucey & Conroy (2015), based on a lensing analysis of low-redshift ETGs.

Previous works of the DM and stellar mass distribution in galaxies have focused on the study of intermediate-luminosity and bright ETGs, with stellar masses $M_\star \gtrsim 10^{10}\,\mathrm{M}_\odot$. At lower mass scales, most of the analysis have assumed universal IMF: e.g. Geha, Guhathakurta & van der Marel (2002), who have fitted long-slit spectroscopy for six dwarf ellipticals (dE), Ryś, van de Ven & Falcón-Barroso (2014), who have performed the full dynamical modelling of 2D kinematic data of 12 dEs, Toloba et al. (2014), who use virial theorem to model effective velocity dispersion for a sample of 39 dEs. In contrast, there are very few analysis of the IMF, see e.g. the direct constraints in ultrafaint dwarf galaxies around the MW (Geha et al. 2013). Moreover, to date, no detailed dynamical analysis has been performed to characterize both the DM content and IMF normalization (i.e. the stellar mass-to-light ratio normalized to that expected for an MW-like distribution) at these low masses, e.g. in dEs. As more massive ETGs, dEs are an ideal target for this kind of study, as they are dominated by old halo stars, have negligible star formation rate at present, and little dust content (de Looze et al. 2010; Toloba et al. 2012, 2014), making the computation of mass-to-light ratios less affected by systematics.

In this paper, we fill the abovementioned gap, studying the central mass distribution of 39 Virgo dEs, drawn from Toloba et al. (2014, hereafter T+14), in the stellar mass range $\sim 10^8 - 10^9\,\mathrm{M}_\odot$. We fit the central dynamics using various (stellar and DM) mass distribution profiles, comparing our findings with results for massive systems. The layout of the paper is the following. In Section 2.1, we describe the data sample and our dynamical method. In Section 3, we discuss the results of the paper. Conclusions are drawn in Section 4.

2 SAMPLES AND DATA ANALYSIS

2.1 Data set

We analyse a sample of 39 dEs in the magnitude range $-19 < \mathrm{M_r} < -16$, selected from the Virgo Cluster Catalog (VCC; Binggeli, Sandage & Tammann 1985) to have high surface brightness with respect to the dwarf galaxy population (Janz & Lisker 2009). Albeit incomplete in luminosity, this sample is representative of the early-type population in this magnitude range (T+14).

The analysis relies on the following data.

(i) The *H*-band structural parameters (the major-axis effective radius, $R_{\rm maj}$, Sérsic index, n, and axis ratio, q) are taken from T+14 and Janz et al. (2014). The nucleus, if present, is excluded from the fit. As noted by Janz et al. (2014), while the global profiles of most galaxies are well approximated by a single Sérsic profile, a more detailed inspection reveals some significant deviations from a single component. For this reason, to analyse systematics in the modelling of the light profile, we have also investigated the impact of both single- and double-Sérsic fits on our results (see Section 3).

(a) *Single Sérsic fit.* The structural parameters are taken from table 4 of T+14, where the $R_{\rm e}$ from the growth curve fit and the Sérsic index from the single Sérsic fit are from Janz et al. (2014). The $R_{\rm e}$s of the growth-curve fits match reasonably well those from direct single-Sérsic fits. For nine systems without a measured value of n (as they had no fit with a single Sérsic component or are not present in Janz et al. 2014), we have adopted $n = 1$, testing the impact for different choices of this parameter (see Section 3). Although only 8 out of the 39 SMAKCED dEs are best fitted with a single (relative to a double) Sérsic profile (see below), to allow us a more homogeneous comparison with massive ETGs from the SPIDER sample (La Barbera et al. 2010), we adopt single-component parameters as our reference case throughout this work.

(b) *Double Sérsic fit.* Data for the inner and outer Sérsic components are taken from table 5 in Janz et al. (2014), for the 33 (out of SMAKCED sample of 39) dEs analysed in that work. Out of these 33 dEs, 25 objects are better described by multiple components, with 19 galaxies being described by a double Sérsic fit and 6 by a single Sérsic profile plus a lens.

(ii) Effective velocity dispersions, $\sigma_{\rm e}$, computed within an ellipse of semimajor axis length of one $R_{\rm maj}$ (T+14). The $\sigma_{\rm e}$s have been computed by T+14 by flux-averaging both rotation velocity and velocity dispersion within each galaxy isophote, hence accounting for both ordered and random motions in each system.

(iii) Age and metallicity estimates are taken from table 5 of T+14, which have fitted relevant Lick spectral indices – measured within the $R_{\rm maj}$ ellipse – with Vazdekis et al. (2012) simple stellar population (SSP) models. Using exponentially declining star formation histories, T+14 have demonstrated that the stellar masses are, on average, fairly consistent with the SSP estimates, but the scatter is larger. For four galaxies (VCC 0170, VCC 0781, VCC 1304 and VCC 1684) Hβ and/or Hα are found in emission. The emission lines are narrower than absorption lines, thus the two components can be decoupled (see Toloba et al. 2014 for details). Although they do not find any significant emission in any of the other galaxies, they cannot rule out the possibility of them having some emission. Thus, for galaxies with undetected emission features the estimated ages (and stellar masses) would be taken as upper limits. See Section 3.1 for further details.

2.2 Analysis

For each galaxy, we obtain the stellar *H*-band mass-to-light (M/L) ratio, $\Upsilon_{\rm SSP}$, using the best-fitted age and metallicity from T+14, and the SSP models of Vazdekis et al. (2012), for a Kroupa IMF. These $\Upsilon_{\rm SSP}$ are converted to those for a Chabrier IMF, by subtracting 0.05 dex (i.e. the difference in normalization between the Kroupa and Chabrier IMFs; Tortora et al. 2009). Under the assumption of a radially constant $\Upsilon_{\rm SSP}$, the deprojected mass profile of the stellar component is written as $\mathrm{M}_*(r) = \Upsilon_* j_*(r)$, with $\Upsilon_\star = \Upsilon_{\rm SSP}$. To derive the light profile $j_*(r)$, we perform a deprojection, under the assumption of spherical symmetry, of the *H*-band Sérsic profiles (from the galaxy structural parameters, see above). Dynamical (DM + light) mass estimates are obtained by fitting the observed $\sigma_{\rm e}$ with spherical, isotropic, Jeans equations (Tortora et al. 2009). To account for the fact that $\sigma_{\rm e}$ is averaged within an elliptic aperture, while we rely on spherical models, we calculate the 3D velocity dispersion from

Table 1. Mass models adopted in this study. Column 1 reports the label of each model. Columns 2, 3, and 4 list the main model ingredients, while columns 5 and 6 give the corresponding IMF normalization, $\delta_{\rm IMF}$, and DM content, $f_{\rm DM}$, estimates from our dynamical analysis. Median, 16–84th percentiles of the sample distribution and the standard error of the median are shown.

ID	Model	$M_{\rm vir}$–$c_{\rm vir}$	IMF	Results	
(1)	(2)	(3)	(4)	(5) $\log\delta_{\rm IMF}$	(6) $f_{\rm DM}$
NFWf	NFW+Sérsic	M+10 - WMAP5	Free	$0.11^{+0.33}_{-0.27}\pm0.06$	$0.35^{+0.27}_{-0.12}\pm0.04$
NFWf-multi	NFW+2 Sérsic	M+10 - WMAP5	Free	$0.09^{+0.36}_{-0.22}\pm0.06$	$0.38^{+0.27}_{-0.15}\pm0.04$
NFWf-hc	NFW+Sérsic	M+10 - $c_{\rm vir}=20$	Free	$-0.21^{+0.53}_{-0.52}\pm0.13$	$0.72^{+0.21}_{-0.29}\pm0.05$
NFWf-WMAP1	NFW+Sérsic	M+10 - WMAP1	Free	$0^{+0.37}_{-0.30}\pm0.09$	$0.47^{+0.25}_{-0.16}\pm0.04$
NFWf-WMAP3	NFW+Sérsic	M+10 - WMAP3	Free	$0.20^{+0.22}_{-0.21}\pm0.09$	$0.29^{+0.20}_{-0.09}\pm0.04$
NFWf-mild-tan-β	NFW+Sérsic+$\beta=-0.4$	M+10 - WMAP5	Free	$0.20^{+0.31}_{-0.19}\pm0.05$	$0.32^{+0.24}_{-0.10}\pm0.03$
NFWf-strong-tan-β	NFW+Sérsic+$\beta=-1$	M+10 - WMAP5	Free	$0.26^{+0.22}_{-0.21}\pm0.07$	$0.30^{+0.20}_{-0.10}\pm0.04$
NFWf-mild-rad-β	NFW+Sérsic+$\beta=0.4$	M+10 - WMAP5	Free	$0.0^{+0.37}_{-0.28}\pm0.07$	$0.40^{+0.25}_{-0.14}\pm0.04$
cMLf	Constant M/L	–	Free	$0.41^{+0.24}_{-0.23}\pm0.05$	0
MOND1	μ_1+constant M/L	–	Free	$0.06^{+0.25}_{-0.22}\pm0.05$	0
MOND2	μ_2+constant M/L	–	free	$0.20^{+0.24}_{-0.24}\pm0.05$	0
NFWC	NFW+Sérsic	M+10 - $c_{\rm vir}$ free	Chabrier	0	$0.60^{+0.16}_{-0.24}\pm0.04$
cMLC	Constant M/L	–	Chabrier	0	$0.61^{+0.17}_{-0.26}\pm0.04$

the radial Jeans equation at the circularized (geometric) effective radius[1] $R_{\rm e}=\sqrt{q}R_{\rm maj}$. The dynamical (i.e. total) mass distribution of galaxies is computed by adopting either single-component (i.e. a radially constant dynamical M/L) or two-component profiles (i.e. stellar component plus DM halo) with the stellar Υ_* being a free-fitting parameter, or fixed to $\Upsilon_{\rm SSP}$ (in case some other quantity, e.g. concentration, is let free to vary, see the different cases described below).

Thus, after the mass model is chosen and the predicted velocity dispersion, $\sigma_e^J(p)$, from the Jeans equation, is derived, the equation $\sigma_{\rm e}^J(p)=\sigma_{\rm e}$ is solved with respect to the free parameter p.[2] The uncertainties on the best-fitting parameter p and derived quantities are obtained by shifting the input parameters (i.e. $\sigma_{\rm e}$, $R_{\rm e}$, n, M_*) according to their errors a number of times and considering the distributions of corresponding best-fitting solutions.

2.3 Mass models

We rely only on velocity dispersions measured within a single aperture, which does not allow us to constrain the shape of the DM profile in detail. To this effect, we explore a variety of models, analysing several plausible assumptions.

The range of models considered in this study are summarized in Table 1. Numerical collisionless *N*-body simulations have provided clues on the formation and the evolution of DM haloes, finding that the DM density of the haloes (from dwarf galaxies to clusters) is independent of halo mass and well described by a double power-law relation with a cusp at the centre (Navarro, Frenk & White 1996, 1997; Moore et al. 1998). Thus, it is a natural choice to start from this theoretical motivated class of DM profiles.

As reference case, we adopt the two-component mass profile NFWf (see Table 1), given by a Sérsic-based stellar mass distribution (with $p\equiv\Upsilon_*$ as a free parameter) and a standard DM halo with a Navarro et al. (1996, hereafter NFW) density profile. We relate virial mass, $M_{\rm vir}$, to concentration, $c_{\rm vir}$, with the mean trend for a *WMAP5* cosmology (for relaxed haloes in Macciò et al. 2008), while the $M_{\rm vir}$–M_* relation is assumed from Moster et al. (2010, M+10 hereafter), which extends down to stellar masses of $\sim10^8\,{\rm M}_\odot$.

The model NFWf-multi is used to study the impact of varying the parametrization of the galaxy light distribution. For galaxies whose light distribution is better fitted by a multiple, rather than a single, component according to Janz et al. (2014), we describe the stellar component with double-Sérsic fit parameters.

Following Tortora et al. (2014b), we also explore how our results depend on the assumed $c_{\rm vir}$– $M_{\rm vir}$ relation. In particular, since for higher mass galaxies (than those analysed in this work), some studies suggest higher concentrations than those from simulations (Buote et al. 2007; Leier, Ferreras & Saha 2012, hereafter LFS12), we also consider 'high-concentration' models (NFWf-hc), with $c_{\rm vir}=20$, in contrast to the typical value of $\sim$12 predicted for our dEs from the (Macciò et al. 2008) relation (for $M_\star\sim10^9\,{\rm M}_\odot$ and $M_{\rm vir}\sim10^{11}\,{\rm M}_\odot$). We refer to these models as 'high-concentration' NFW models, NFWf-hc. Moreover, the impact of cosmological framework on the theoretical $c_{\rm vir}$–$M_{\rm vir}$ relation is analysed with models NFWf-WMAP1 and NFWf-WMAP3, which use *WMAP*1 and *WMAP*3 results from *N*-body simulations in Macciò et al. (2008). Notice that *WMAP*1 predictions are very similar to the $c_{\rm vir}$–$M_{\rm vir}$ based on the first release of Planck cosmological parameters (Dutton & Macciò 2014).

A possible source of systematics is the hypothesis of isotropic stellar orbits, as spatially resolved stellar kinematics for a handful of dEs has been found to be better modelled with tangential anisotropies, rather than isotropy (e.g. Geha et al. 2002). Although a detailed analysis of galaxy anisotropies is far from being trivial, and is certainly beyond the scope of this work, we have estimated the impact of anisotropy on our inferences. To this effect, in our list of models (Table 1), we have also included three cases corresponding to radially constant anisotropy β in the Jeans equations (see also Tortora et al. 2009, 2012): a 'mild' tangential anisotropy, $\beta=-0.4$, (NFWf-mild-tan-β), a 'strong' tangential anisotropy, $\beta=-1$,

[1] This circularized quantity is used throughout this work.
[2] The adopted galaxy models and the parameter p are defined in Section 2.3.

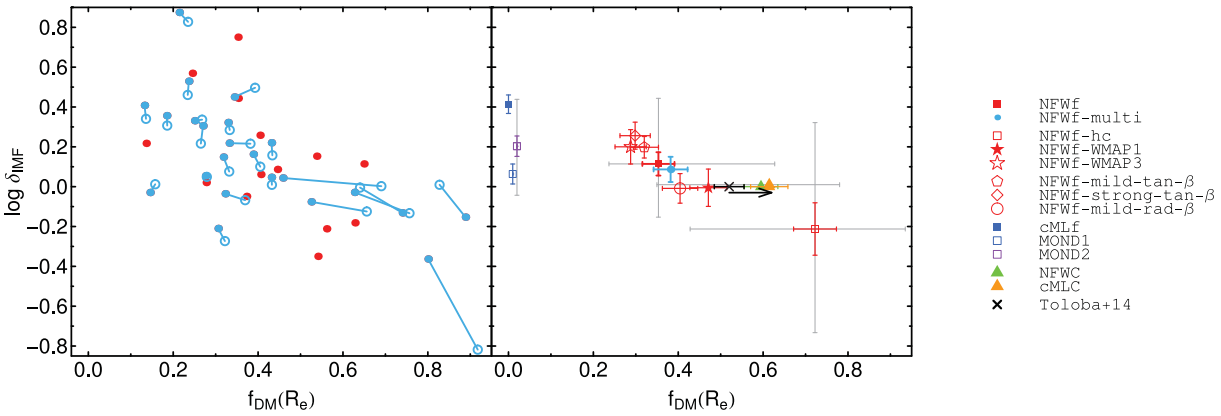

Figure 1. IMF normalization, δ_{IMF}, versus effective ($< 1 R_e$) DM fraction, f_{DM}. Left-hand: results of the NFWf model for individual galaxies. For systems with no Sérsic index available from Janz et al. (2014), we plot the range of values found if n is varied from 0.5 to 2 (dark-green curves). Cyan symbols correspond to galaxies with either a single (dots) or double-Sérsic (open circles) fit available. Different cyan symbols are connected by cyan lines to highlight the effect of changing the parametrization of the light profile on our results. Red points are for galaxies for which only single–fit parameters are available. Right-hand: medians and standard errors of the median are plotted for different models (see Table 1): NFWf (filled red square), NFWf-multi (cyan dot), NFWf-hc (open red square), NFWf-WMAP1 (filled red star), NFWf-WMAP3 (open red star), NFWf-mild-tan-β (open red pentagon), NFWf-strong-tan-β (open red diamond), NFWf-mild-rad-β (open red circle), cMLf (filled blue square), MOND1 (open blue square), MOND2 (open violet square), NFWC (green triangle), and cMLC (orange triangle). For a few representative models, the 16–84th quantiles of the distributions are also shown as grey error bars. The median f_{DM} and the standard errors of the median from T+14 are shown as a black cross and error bars, and the change after uniforming the definition for M_{dyn} and M_* to ours is outlined with a black horizontal arrow. Legend for the symbols plotted in the right-hand panel is also shown.

(NFWf-strong-tan-β), and a 'mild' radial anisotropy, $\beta = 0.4$ (NFWf-mild-rad-β).

To further explore the effect of mass modelling, as well as the impact of adopting alternative theories of gravity on our results, we also consider the following models.

(i) cMLf. In contrast to the DM haloes predicted by N-body simulations, a different class of models relies on the assumption that total mass follows the light distribution, i.e. constant M/L models with $\rho_{M/L} = \Upsilon_{tot} j_*$. Thus, we adopt a no-DM model with constant M/L profile, defined to have a total mass distribution $\rho_{noDM} = \Upsilon_* j_*$, with Υ_* as the only free-fitting parameter.

(ii) MOND. A modified Newtonian gravitational acceleration model, in the regime of low acceleration, according to the MOND theory (Milgrom 1983; Begeman, Broeils & Sanders 1991), has become an alternative theory to reproduce galactic dynamics without DM. The acceleration as a function of the radius r, $g(r)$, is given by $g(r)\mu(x) = g_N(r)$, where $x = g(r)/a_0$, a_0 is the MOND acceleration constant (which sets the transition from the Newtonian to the low-acceleration regime), g_N is the Newtonian acceleration, and $\mu(x)$ is an empirical function interpolating between the two regimes. We adopt the following expressions: (a) $\mu_1(x) = x/(1+x)$ (MOND1, Famaey & Binney 2005; Angus 2008) and (b) $\mu_2(x) = x/\sqrt{1+x^2}$, which has been the first one successfully tested with observations (MOND2, Sanders & McGaugh 2002). A constant M/L profile with a free Υ_* is adopted for the total mass distribution (see Tortora et al. 2014a for further details).

To complete our large model portfolio, we also adopt two models with $\Upsilon_\star = \Upsilon_{SSP}$, with a fixed Chabrier IMF normalization:

(i) NFWC. An NFW model, adopting the same M_{vir}–M_* relation used for NFWf, but dismissing the $c_{vir}-M_{vir}$ relation, and leaving c_{vir} as a free parameter.

(ii) cMLC. A total mass distribution with radially constant M/L, but setting $\Upsilon_\star = \Upsilon_{SSP}$. The total M/L is left free to vary. This model is characterized by a radially constant DM fraction.

The final products of our analysis are the SSP M/L, Υ_{SSP}, the dynamically determined stellar and total M/Ls, Υ_* and Υ_{dyn}, the inferred mismatch parameter δ_{IMF} (for models with free IMF normalization), defined as $\delta_{IMF} \equiv \Upsilon_\star/\Upsilon_{SSP}$, and effective DM fraction, $f_{DM} \equiv 1 - \Upsilon_\star/\Upsilon_{dyn}$.

3 IMF MISMATCH AND DM FRACTIONS

In Fig. 1, we plot the results of our analysis. In the left-hand panel, we plot δ_{IMF} versus f_{DM} for our reference NFWf model (cyan symbols), while the median δ_{IMF}, computed for the whole sample of dEs, versus the median f_{DM}, are shown in the right-hand panel, for all models listed in Table 1 (error bars show the 16–84th percentile scatter in the data). For the 'standard' NFWf, in two cases (i.e. VCC 0009 and VCC 1355) the model fails to fit the data. Only 50 per cent of the sample is fitted by the 'high-concentration' model, NFWf-hc. For NFWf-WMAP1, VCC 0009 is the only galaxy for which the model fails, while for NFWf-WMAP3 the model fails for VCC 0009, VCC 0170, VCC 0308 and VCC 1355. The 'fixed IMF' models (NFWC and cMLC) only fail for VCC 1910. On the other hand, MOND and cMLf models allow all galaxies to be fitted. The two-component (or Chabrier IMF-fixed) models fail to reproduce the data as the mass from the assumed DM model (or from the Chabrier IMF-based model) is larger than the total mass allowed by the observed σ_e. This is not contemplated in the cMLf and MONDian models, for which it is always possible to find a Υ_* reproducing the data.

In the next sections, we will discuss the δ_{IMF} and f_{DM} estimates for each galaxy in the sample and then we will study the impact of mass model comparing the median and the standard error of the median[3]

[3] In statistics, the standard error of the mean tells how accurate the estimate of the mean is likely to be, and it is different from the standard deviation of a set of data. A similar definition can be made for the median, and in particular, it can be shown that the standard error of the median is obtained

calculated over the sample distribution of the models in Table 1. We also determine the 16–84th percentiles of the distributions.

3.1 NFW and systematics in light profile

Our reference NFWf model produces, on average, $\delta_{\rm IMF} \sim 1.3$ (log $\delta_{\rm IMF}\sim$0.1 dex) and $f_{\rm DM} \sim 0.35$. The large scatter in $\delta_{\rm IMF}$ (see points in the left-hand panel and grey scatter bar in the right-hand panel of Fig. 1) is due to the fact that while most galaxies turn out to have an IMF normalization consistent with an MW-like distribution (log $\delta_{\rm IMF}\sim$0), a significant fraction of them ($\sim$30 per cent) have a super-Salpeter IMF normalization (i.e. $\delta_{\rm IMF} > 1.8$). DM fractions are, on average, in the range $\sim$0.2–0.6, consistent with independent estimates for 'normal' (as opposite to dwarf) ETGs (see below). The standard error of the median is $\sim$0.04 for $f_{\rm DM}$ and $\sim$0.05 dex for $\delta_{\rm IMF}$.

Adopting 10 per cent uncertainties on $R_{\rm e}$ and n, and propagating the uncertainties on age and metallicity from table 5 in T+14, we find 1σ average errors on $\delta_{\rm IMF}$ and $f_{\rm DM}$ of $\sim$0.15 dex and $\sim$0.05, respectively. Taking the uncertainties into account, we find that some dEs have $\delta_{\rm IMF}$ inconsistent (heavier than) a Chabrier IMF normalization. In particular, at the 3σ level, the galaxies VCC0397, VCC0750, and VCC1684 have $\delta_{\rm IMF} > 1.8$, while VCC0523, VCC0781, VCC1122, and VCC1528 have $\delta_{\rm IMF} > 1$ (but $<$1.8). Assuming 30 per cent (rather than 10 per cent) uncertainties on both $R_{\rm e}$ and n, the error on $\delta_{\rm IMF}$ is almost unchanged, while for $f_{\rm DM}$ is of $\sim$0.1 and we find that, at 3σ, VCC0750 and VCC1684 still have $\delta_{\rm IMF} > 1.8$, while VCC0397 and VCC0781 have $1 < \delta_{\rm IMF} < 1.8$. Note that to these larger $\delta_{\rm IMF}$ correspond smaller DM fractions, with $f_{\rm DM} \sim 0.2$–0.3. Thus, while for most galaxies our results are consistent with an MW-like normalization, our analysis suggests that for at least a few dEs, the M/L detected from previous studies (e.g. T+14) might be partly accounted for by heavier IMF normalization, rather than large DM fractions in the galaxy central regions.

Note that a $\delta_{\rm IMF}$ larger than one can be due to either a bottom-heavy (due to a larger fraction of dwarf relative to giant stars) or a top-heavy IMF (because of the large fraction of stellar remnants from evolved massive stars). This degeneracy has been broken in ETGs, by studying gravity-sensitive features in the integrated light of galaxies. Such spectroscopic approach allows one to constrain the mass fraction of dwarf-to-giant stars in the IMF, rather than its overall normalization, in contrast to dynamical and lensing methods (Conroy & van Dokkum 2012; Spiniello et al. 2012; La Barbera et al. 2013). Indications of top-heavy IMFs are found from (a) galaxy number counts (Baugh et al. 2005), (b) in ultracompact dwarfs, based on the large fraction of low-mass X-ray binaries found (Dabringhausen et al. 2012), (c) in the MW centre (e.g. Bartko et al. 2010) or (d) in Galactic globular clusters (e.g. Prantzos & Charbonnel 2006). In addition, galaxy formation models reproduce the observed intracluster medium if a top-heavy IMF is adopted (Nagashima et al. 2005). Studies of gravity-sensitive features in dEs are still missing, thus, we cannot exclude a top-heavy IMF in these systems.

As mentioned in Section 2.1, Sérsic indices are measured only for 30, out of 39, dEs analysed in this work. For systems with no available n, we have adopted $n = 1$. To test the effect of this assumption, we have varied the Sérsic n from 0.5 to 2, which is a 'conservative' range, encompassing the observed values, for the SMAKCED sample of dEs. For the seven (out of nine) systems where the NFWf fits do not fail, the impact of changing the n is shown in the left-hand panel of Fig. 1 (see dark-green lines), which show how the $\delta_{\rm IMF}$ and $f_{\rm DM}$ values change when the n is varied. Larger Sérsic indices correspond to smaller $\delta_{\rm IMF}$ and larger $f_{\rm DM}$. We find, on average, a mild variation of $\sim\pm$ 0.05 dex on both $\delta_{\rm IMF}$ and $f_{\rm DM}$, with negligible impact on median values for the whole sample. We have further tested the effect of the $n = 1$ assumption on the galaxies with a measured Sérsic index, by varying it to $n = 1$. On average, the variation is 0.03 for $f_{\rm DM}$ and -0.02 dex for $\delta_{\rm IMF}$.

We have also tested the impact of different parametrization of the light on our dynamical estimates. The model NFWf-multi replaces the single Sérsic profile with the double Sérsic parametrization for those systems which are better fitted by the latter model. The results over the whole sample for both NFWf and NFWf-multi models are plotted in the left-hand panel of Fig. 1, to highlight the effect of a refined description of the light distribution in our dynamical analysis. The galaxies with the largest $f_{\rm DM}$ are the most affected. However, the medians computed over the whole sample are almost unchanged with respect to the reference NFWf (see right-hand panel of Fig. 1).

As we have mentioned in Section 2.1, galactic nuclei, if present, are excluded in the fit of the light distribution of the SMACKED dEs. It is important to quantify the impact on our results if these nuclei are included in the analysis. Because it is not trivial to extract the amount of light due to the nuclei from T+14, we rely on estimates from independent literature. 9 out of the 39 galaxies are shared with Paudel, Lisker & Kuntschner (2011), who has provided estimates of nuclear fluxes, $f_{\rm nuc}$, at $r < 2$ arcsec and total ones, $f_{\rm tot}$ (their Table 1), finding that the nuclei account for $<$2 per cent of the total flux. Assuming that this limit can be extended to the whole SMAKCED sample, we have included in our modelling procedure a constant mass distribution with flux $f_{\rm nuc}$ at $r < 2$ arcsec. We find that the impact on our results is negligible, since the $\delta_{\rm IMF}$ gets smaller by 0.02 dex, while the $f_{\rm DM}$ are left unchanged. The $\delta_{\rm IMF}$ would get smaller by more than 0.1 dex for nuclei which account for more than 10 per cent of the total flux. However, such prominent nuclei are not observed.

Finally, correcting for not detected emission lines would make the ages and stellar masses smaller, getting $f_{\rm DM}$ and $\delta_{\rm IMF}$ larger. To provide a quantification of this effect we have augmented the measured $H\beta$ index by its error (which we use to estimate the impact of emission), and matched it with Vazdekis et al. (2012) model predictions, deriving younger stellar populations. We have also taken into account metallicity change due to age variation, using the model predictions on the [Mg/Fe]$'$–$H\beta$ plane. On average, stellar masses and $\delta_{\rm IMF}$ get smaller and larger by $\sim$0.05 dex, respectively, and $f_{\rm DM}$ is larger by $\sim$0.07.

3.2 DM mass model degeneracy

We start discussing the impact of different $c_{\rm vir}$–$M_{\rm vir}$ relations. We notice that for 'high-concentration' NFW models, NFWf-hc, the best-fitting Υ_* is significantly lower than that for a Chabrier IMF (i.e. $\delta_{\rm IMF}<1$). As already discussed, a value as high as $c_{\rm vir} = 20$ is able to describe only $\sim$50 per cent of the SMAKCED dEs. These models predict too much mass in the centre than what is allowed by the measured $\sigma_{\rm e}$. Together with the fact that the Chabrier IMF gives the minimum normalization with respect to either top- or bottom-heavier distributions (when other relevant stellar population parameters, such as age and metallicity, are fixed), this result

by multiplying the standard error of the mean by the factor 1.253 (Harding, Tremblay & Cousineau 2014).

suggests that high-concentration models are generally disfavoured for SMAKCED dEs. Since only 50 per cent of the sample is fitted, the standard errors of the median get higher, i.e. ∼0.05 for $f_{\rm DM}$ and ∼0.13 dex for $\delta_{\rm IMF}$. For what concerns different theoretical predictions for the $c_{\rm vir}$–$M_{\rm vir}$ correlation, we have analysed the impact of different cosmologies (*WMAP*1 versus *WMAP*3 versus *WMAP*5). We find that within a *WMAP*1 cosmology, which predicts larger concentrations with respect to *WMAP*5, $\delta_{\rm IMF}$ gets smaller (∼1), and DM fraction larger than the *WMAP*5 case. In contrast, a *WMAP*3 cosmology, because of smaller concentrations, gives larger $\delta_{\rm IMF}$ and smaller DM fractions (see Fig. 1).

The right-hand panel in Fig. 1 illustrates the effect of anisotropy on our sample results (see open red symbols), with respect to our reference NFWf model (filled red square). For tangential anisotropy (e.g. Geha et al. 2002), we obtain larger dynamical masses (see also Tortora et al. 2012), larger $\delta_{\rm IMF}$ and smaller $f_{\rm DM}$ with respect to the NFWf isotropic case. In particular, for $\beta = -0.4$ ($\beta = -1$) $\delta_{\rm IMF}$ gets larger by ∼0.09 (∼0.15) and $f_{\rm DM}$ is smaller by ∼0.03 (∼0.05). For the sake of completeness, we also consider here results when radial anisotropy is assumed. This provides smaller $\delta_{\rm IMF}$ (by ∼0.11) and larger DM content (by ∼0.05). Overall, we conclude that the effect of anisotropy is not negligible, especially for what concerns $\delta_{\rm IMF}$, while for $f_{\rm DM}$ the results remain constrained within the typical error budget of our models, even with the more 'extreme' assumption (e.g. $\beta = -1$).

The highest $\delta_{\rm IMF}$ are obtained, as expected, by the model with no DM, i.e. cMLf (filled blue square and error bar in Fig. 1), where $\delta_{\rm IMF}$ is significantly larger than the NFWf case ($\delta_{\rm IMF} > 1.5$), with ∼80 per cent of galaxies nominally consistent with a super-Salpeter IMF normalization. When assuming tangential anisotropy, all galaxies in this model would turn out to have super-Salpeter normalization.

For what concerns models with modified gravity, median results are shown in Fig. 1 as open blue (MOND1) and violet squares (MOND2), respectively. The $\delta_{\rm IMF}$s differ by ∼0.14 dex between the two cases, bracketing results for the NFWf. However, within uncertainties the two models give consistent results. Thus, for dEs we confirm the same conclusions as for more massive ETGs, i.e. that the MOND and DM frameworks are equivalent to reproduce the dynamics of the central galaxy regions (Tortora et al. 2014a).

Finally, Fig. 1 shows $f_{\rm DM}$ estimates for the two models with fixed Chabrier IMF, i.e. NFWC and cMLC, respectively. As expected, because of the intrinsically lower stellar M/L normalization, the $f_{\rm DM}$ are much larger ($\gtrsim 0.4$, with an average of ∼0.6) than the NFWf model.

3.3 Comparison with literature

As a comparison with independent results, Fig. 1 also plots $f_{\rm DM}$ estimates from table 8 of T+14 (black cross and arrow in the right-hand panel in Fig. 1). They adopt a Kroupa IMF to describe the stellar component and use the virial relation $M_{\rm dyn} \propto K(n)\sigma^2 R_{\rm e}$, with $K = 3.63$, corresponding to a Sérsic profile with $n \sim 2$ (Cappellari et al. 2006). After correcting their stellar masses to a Chabrier IMF, we obtain a median $f_{\rm DM}$ value of $0.52^{+0.16}_{-0.15}$, which can be compared with our results for the cMLC model. A difference of $\Delta f_{\rm DM} \sim 0.1$ is found (see Fig. 1). This discrepancy is due to the fact that (1) T14 adopt a different definition, with respect to our work, for the total and stellar mass within 1 $R_{\rm e}$, as dynamical masses are estimated within a sphere with radius $R_{\rm e}$ (following the virial definition), while stellar masses are calculated within a projected cylinder with radius $R_{\rm e}$; (2) the average Sérsic index of the T14 sample is $n \sim 1.5$, and not $n \sim 2$ (as they assume to compute the $K(n)$). Note that the $K(n)$ tends to decrease with n (Bertin, Ciotti & Del Principe 2002). Correcting for these different assumptions, $M_{\rm dyn}$ become larger and stellar masses within 1 $R_{\rm e}$ are smaller, making the median $f_{\rm DM}$ value larger and identical to our cMLC estimate (this effect is outlined by the black horizontal arrow in the right-hand panel in Fig. 1). This agreement is expected if the same data and mass model are adopted.

We have also performed a comparison of our cMLC $f_{\rm DM}$ with the values derived by means of a complete Jeans dynamical modelling (JAM) of the 2D kinematics in Ryś et al. (2014). After the cross-matching, six galaxies are left. Looking at their face values, Ryś et al. (2014) $f_{\rm DM}$ are, on average, larger by ∼0.1. These JAM values look quite similar to the virial predictions, which assume the same K-value of massive ETGs in Cappellari et al. (2006). If we normalize these mass definitions to our cMLC model, the discrepancy is even larger (by ∼0.2). However, we find that this discrepancy is possibly related to inhomogeneity between the SMAKCED and Ryś et al. (2014) data sets as differences in (a) wavebands used to calculate structural parameters and M/L (H-band in SMAKCED versus r-band in Ryś et al. 2014), (b) stellar mass determinations, since absorption lines are fitted with Vazdekis et al. (2012) models in SMAKCED survey and colour-to-Υ_* formula from Bell et al. (2003) is used in Ryś et al. (2014), and (c) estimated velocity dispersions. A complete understanding of these sources of systematics is beyond the scope of this work.

3.4 Comparison with massive ETGs

In this section, we discuss our results for dEs into the broader framework of the continuity of intrinsic properties of spheroidal systems, comparing the finding for dEs with those for a local ($0.05 < z < 0.095$), complete, sample of ∼4300 giant ETGs drawn from the SPIDER survey (see La Barbera et al. 2010 and Tortora et al. 2012 for further details about sample selection). The SPIDER data set includes stellar masses derived from the fit of stellar population synthesis (SPS) models to optical+near-infrared photometry[4] (Swindle et al. 2011), galaxy structural parameters (effective radius $R_{\rm e}$ and Sérsic index n; using 2DPHOT, La Barbera et al. 2008), homogeneously derived from g through K wavebands, and SDSS central-aperture velocity dispersions, $\sigma_{\rm Ap}$. SPIDER ETGs are defined as luminous bulge dominated systems, featuring passive spectra in the central SDSS fibre aperture (La Barbera et al. 2010). The dynamical analysis, presented in our previous papers for SPIDER ETGs (Tortora et al. 2013; Tortora et al. 2014b), is similar to that carried out for dEs in this work. In particular, we have derived DM content and IMF normalization for SPIDER ETGs using the NFWf profile, i.e. assuming the NFW+Sérsic profile, with the same $c_{\rm vir}$–$M_{\rm vir}$ and M_*–$M_{\rm vir}$ relations as for dEs.

The results for dE and luminous ETGs are compared in Fig. 2, where $R_{\rm e}$ and $\sigma_{\rm e}$ are plotted as a function of M_* (see also T+14), and colour-coded in terms of $\delta_{\rm IMF}$ and $f_{\rm DM}$ (left-hand and right-hand panels), respectively. The figure shows the well-known shallower $R_{\rm e}$–M_* and $\sigma_{\rm e}$–M_* relations for dEs, with respect to the relations for luminous ETGs (Matković & Guzmán 2005; Woo, Courteau & Dekel 2008; Toloba et al. 2012). Note that dEs have an almost constant $R_{\rm e}$ with respect to M_*, with no dependence of $\delta_{\rm IMF}$ on

[4] Note that these stellar masses are consistent with ones obtained adopting absorption lines (Swindle et al. 2011).

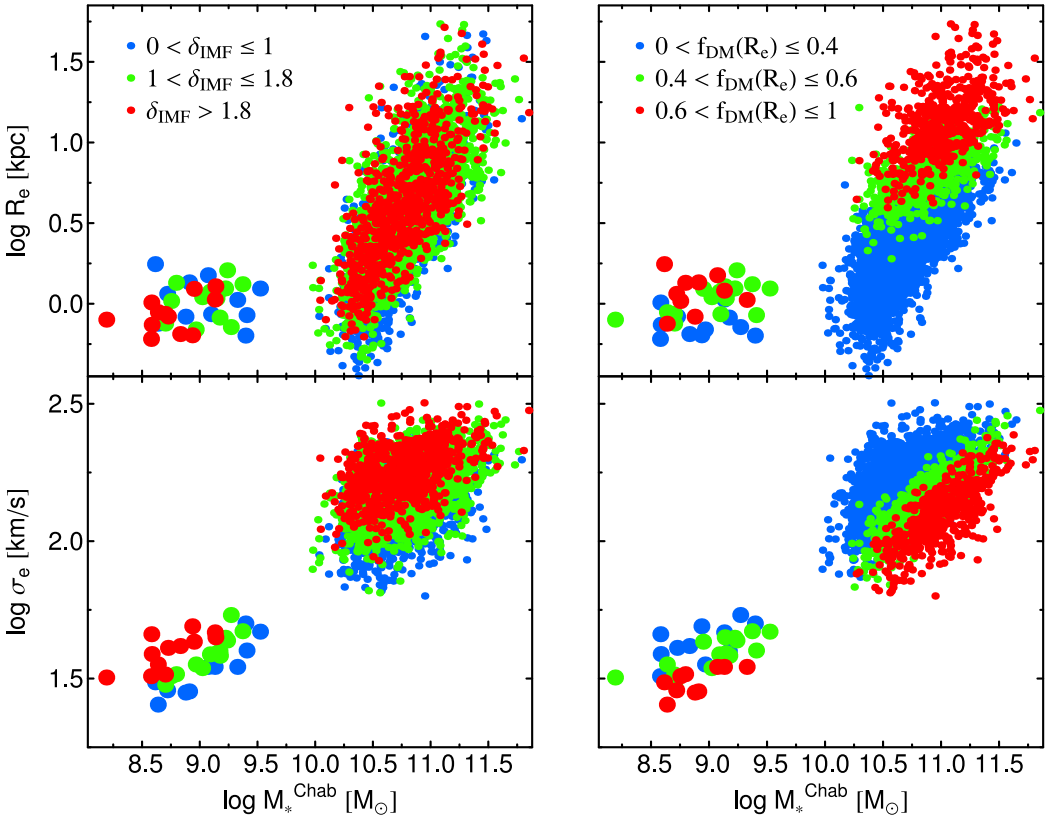

Figure 2. Effective radius (top) and galaxy velocity dispersion (bottom panels) versus M_*^{Chab}. Different points are colour-coded according to δ_{IMF} (left-hand panels) and f_{DM} (right-hand panels), respectively (see labels in the top panels). The model NFWf is adopted. Large and small dots correspond to SMAKCED dEs and bright SPIDER ETGs, respectively. Structural parameters for the SPIDER ETGs have been measured in the *K* band, roughly matching the *H*-band photometry of SMAKCED dEs.

R_e at fixed stellar mass (see big dots with different colours in the top-left panel of Fig. 2). On the contrary, in the σ_e–M_* plot (bottom–left panel), larger δ_{IMF} correspond to larger σ_e. Notice that this is expected in our one-parameter NFWf models, as dEs have almost constant R_e, and at fixed M_* the only way to match a higher σ_e is thus to have a larger (smaller) δ_{IMF} (f_{DM}, see bottom-right panel). For what concerns the behaviour with f_{DM} (right-hand panels of the figure), we also notice that both dEs and luminous ETGs have effective DM fractions driven by R_e, since bigger galaxies have larger f_{DM} (see also Napolitano, Romanowsky & Tortora 2010; Tortora et al. 2012).

The trends of δ_{IMF} and f_{DM} with M_* and σ_e are plotted more explicitly for dEs and luminous ETGs, in Fig. 3 (red and black symbols, respectively). The δ_{IMF} (f_{DM}) appears to increase (decrease) with σ_e (panels a and c) consistent with what seen in Fig. 2, while no significant correlation of both f_{DM} and δ_{IMF} is seen with M_*^{Chab} (panels b and d). However, we remind the reader that although representative of the population of dEs, SMAKCED sample is certainly incomplete with respect to M_* and σ_e. Further analysis, based on spatially extended kinematical data (i.e. 2D spectroscopy) and complete galaxy samples, are required to pinpoint the intrinsic correlations of DM and IMF normalization with galaxy parameters in dEs.

For what concerns median values of δ_{IMF} and f_{DM} (red dots and error bars in Fig. 3), we see that in the δ_{IMF}–M_* diagram (panel b), the median δ_{IMF} for dEs is consistent, overall, with that for ETGs. This is due to the fact that while most dEs have δ_{IMF} consistent with an MW-like normalization, a significant fraction of them exhibit a Salpeter or super-Salpeter normalization (Section 2.1). In fact, when looking at the δ_{IMF}–σ_e plot (panel (a)), we see that dEs tend to have, on average, slightly higher IMF normalization than the lowest σ_e ETGs (whose normalization is fully consistent with the MW-like distribution). Interestingly, the trend of f_{DM} with M_* (panel d) points to a double-value behaviour of DM content with stellar mass in ETGs, with larger f_{DM} in most massive ETGs ($M_\star \gtrsim 10^{11}\,M_\odot$) and dEs ($M_\star \sim 10^9\,M_\odot$), and a minimum at $M_\star \sim 10^{10}\,M_\odot$.

To have some further hints of the f_{DM} trends, we have constructed toy mass models, based on our reference NFWf model by computing stellar mass profiles according to either a Chabrier or a Salpeter IMF, and adopting the mean size- and *n*–mass relations of dEs and massive ETGs, respectively. Results for the f_{DM} trends are shown in the bottom panels of Fig. 3. At fixed IMF, such toy models predict a double-value trend for the f_{DM} as a function of both σ_e and M_*^{Chab} (panel c and d). In the $f_{DM} - M_\star$ diagram (panel d), this trend matches quite well the observations for both dEs and ETGs. In contrast, for the $f_{DM} - \sigma_e$ diagram, the toy models give a good match to dEs (although some overall variation of δ_{IMF} is required to exactly match the trend, as also seen in panel a), while there is a clear mismatch in the case of massive ETGs, where toy models predict an increasing trend of f_{DM} while the inferred f_{DM} tends to mildly decrease with σ_e. As seen in panel a, this disagreement is due to the fact that toy models assume a constant IMF normalization, while data imply a strong trend of δ_{IMF} with σ_e. In summary, our toy-models also support a double-value behaviour in the f_{DM}–M_* correlation.

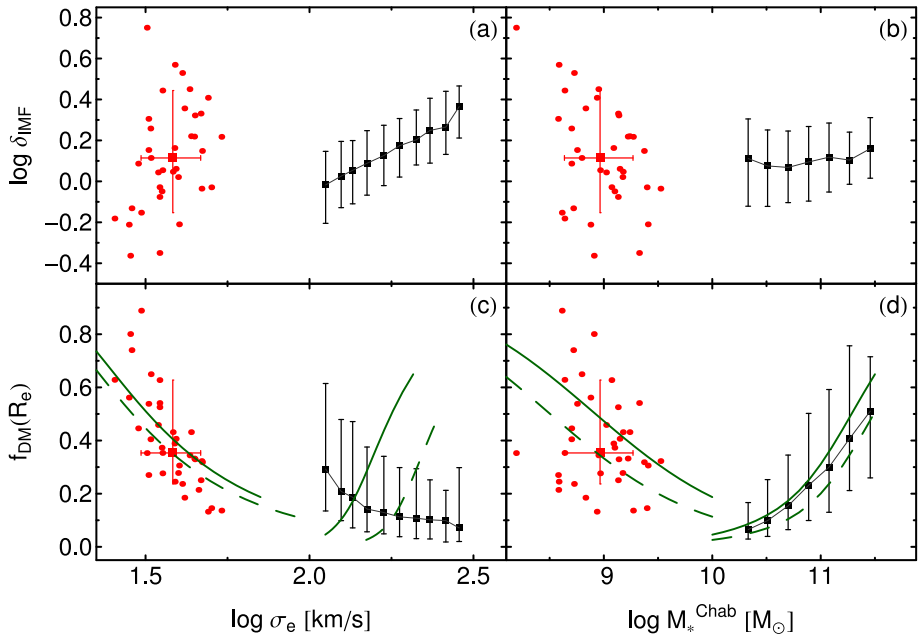

Figure 3. The δ_{IMF} (top) and f_{DM} (bottom) are plotted as a function of galaxy velocity dispersion, σ_e (left-hand) and Chabrier-based stellar mass, M_*^{Chab} (right-hand). Red and black symbols are for dE and SPIDER ETGs, respectively. For the SPIDER sample, only median values with 16–84th quantiles are shown, as black squares with error bars. The red squares and error bars plot median values and 1σ scatter for the sample of dEs (plotted individually as red dots). Green lines are toy models, obtained assuming a NFWf model, and mean size- and n-M_*^{Chab} relations derived, separately, from the two samples. Solid and dashed lines refer to $\delta_{IMF} = 1$ (MW-like) and =1.8 (Salpeter normalization), respectively.

We have also verified that the double-value trend of f_{DM} does not depend critically on our assumptions of a given M_{vir}–M_* relation. In fact, a similar result is found when considering the cMLC model.

The U-shape behaviour of f_{DM} with M_* in early-type systems can be understood as a result of different feedback mechanisms in these systems at different mass scales. In lowest mass galaxies (dEs), star formation is likely inhibited by (e.g.) supernovae feedback. This becomes less important at increasing galaxy mass (Dekel & Birnboim 2006; Cattaneo et al. 2008). However, at the highest M_*, additional processes, such as dry merging, AGN feedback or halo-mass quenching further inhibit gas cooling, and decrease star formation efficiency again (Dekel & Birnboim 2006). Hence, the lowest and highest mass galaxies are expected to have the lowest star formation efficiency, and thus, under the assumption of a universal DM distribution, the highest DM content. The f_{DM} trend in dEs and luminous ETGs adds up to other well-known correlations in ETGs, such as the trends of total M/L and star formation efficiency (Benson et al. 2000; Marinoni & Hudson 2002; van den Bosch et al. 2007; Conroy & Wechsler 2009; M+10), the U-shape of half-light dynamical M/L (Wolf et al. 2010; Toloba et al. 2011), $\mu_e - R_e$ (Capaccioli, Caon & D'Onofrio 1992; Kormendy et al. 2009) and size–mass (Shen et al. 2003; Hyde & Bernardi 2009) relations, the trends of optical colour and metallicity gradients (Kuntschner et al. 2010; Spolaor et al. 2010; Tortora et al. 2010, 2011), as well as DM gradients (Napolitano et al. 2005) with galaxy mass.

4 DISCUSSIONS AND CONCLUSIONS

In this work, we have performed an isotropic Jeans dynamical analysis for 39 dE in the Virgo cluster, from T+14. For the first time, we have studied the IMF normalization and the effective DM content using a suite of fixed DM profiles and the stellar M/L as a free-fitting parameter. We have also performed the analysis with MOND, modified-gravity, models. The main results are shown in Fig. 1 where we find that, on average, using an NFW profile and standard c_{vir}–M_{vir} relation from N-body simulations (NFWf model in Table 1), dEs have[5] $\log \delta_{IMF} = 0.11^{+0.33}_{-0.27}$ with error ∼0.05 dex (i.e. consistent with a Chabrier-like IMF normalization) and $f_{DM} = 0.35^{+0.27}_{-0.12}$ with error ∼0.03. A constant-M/L model, with no-DM content (the cMLf model), maximizes the stellar mass content (i.e. the δ_{IMF}), pointing to super-Salpeter IMF normalizations. In the MOND scenario, using two standard interpolating functions (MOND1, Famaey & Binney 2005; MOND2, Sanders & McGaugh 2002) we find results which encompass the NFW predictions, in agreement with results for massive ETGs (Tortora et al. 2014a). For completeness, we have also analysed the cases of a universal Chabrier IMF (NFWC and cMLC), which provide larger effective DM fractions when compared to our reference model with free IMF normalization, NFWf. The derived DM fractions for the NFWC model are fully consistent with the estimates in Toloba et al. (2014), if stellar and dynamical masses are homogeneously defined. We have also analysed the impact of several further assumption, such as light-profile parametrization, velocity dispersion anisotropy, and assumptions on the c_{vir}–M_{vir} relation. In particular, at the mass scale of dEs, our data seem to disfavour a c_{vir}–M_{vir} relation steeper than that from simulations, as it might be the case for more massive haloes (see Leier et al. 2012), while if tangential anisotropy is assumed (see e.g. Geha et al. 2002), we obtain larger δ_{IMF} and smaller f_{DM} with respect to the reference isotropic case (on the contrary, radial anisotropy produces larger f_{DM} and smaller δ_{IMF}). Although most of dEs have δ_{IMF} consistent with an MW-like normalization, for the reference NFWf model, we also find evidence that some dEs

[5] Median and 16–84th percentiles of the sample distribution are shown, together with the standard error.

might have $\delta_{\rm IMF} > 1$ or >1.8 at high statistical significance, i.e. an IMF which is heavier that a Chabrier- or Salpeter-like distribution.

In Figs 2 and 3, we have compared results for dEs with those for massive ETGs from the SPIDER sample (La Barbera et al. 2010; Tortora et al. 2012, 2013). We find some hints that $\delta_{\rm IMF}$ might increase with $\sigma_{\rm e}$, as in more massive ETGs (Tortora et al. 2013, 2014b). However, spatially extended kinematical data (i.e. 2D spectroscopy) and complete galaxy samples are required to confirm if this trend is real, rather than due to sample incompleteness. Moreover, we find that, on average, dEs tend to have slightly higher IMF normalization than ETGs at lowest $\sigma_{\rm e}$ ($\sim$100 kms^{-1}, whose IMF normalization is fully consistent with an MW-like distribution).

The trend of $f_{\rm DM}$ with M_* suggests a double-value behaviour, with largest $f_{\rm DM}$ in most massive ETGs ($M_\star \gtrsim 10^{11}$ M$_\odot$) and dEs ($M_\star \sim 10^9$ M$_\odot$), and a minimum at $M_\star \sim 2{-}3 \times 10^{10}$ M$_\odot$. These trends mirror those of the dynamical M/L (Wolf et al. 2010; Toloba et al. 2011), and of total star formation efficiency with respect to mass (Benson et al. 2000; Marinoni & Hudson 2002; van den Bosch et al. 2007; Conroy & Wechsler 2009; M+10), which are the result of the interplay among different physical processes, such as SN feedback at lowest galaxy masses, and AGN feedback, galaxy merging, and halo mass heating in the most massive ETGs (Tortora et al. 2010).

In this paper, we have performed a first attempt to constrain, simultaneously, the IMF normalization and dark matter content of low-mass (dwarf) ETGs, finding for at least a few systems that the $\delta_{\rm IMF}$ is heavier than the MW-like value. Since such a 'heavy' $\delta_{\rm IMF}$ could be due to either a bottom- or a top- heavy distribution, a natural follow-up of this work would be to study gravity-sensitive features in the integrated light of galaxies, which have provided, so far, important constraints to the IMF slope of massive ETGs (Conroy & van Dokkum 2012; Spiniello et al. 2012, 2014; Ferreras et al. 2013; La Barbera et al. 2013). In fact, a similar analysis is currently lacking for dEs. In the future, it will be also necessary to apply the present analysis to large and complete samples including a variety of stellar systems, such as dE, dwarf spheroidals, ultracompact dwarfs, and late-type galaxies, to achieve a complete picture of how the dark matter and stellar components have been assembled along the whole galaxy mass sequence.

ACKNOWLEDGEMENTS

We thank the referee for his/her detailed report which has contributed to improve the manuscript. CT has received funding from the European Union Seventh Framework Programme (FP7/2007-2013) under grant agreement no. 267251 'Astronomy Fellowships in Italy' (AstroFIt). FLB acknowledges support from grant AYA2013-48226-C3-1-P from the Spanish Ministry of Economy and Competitiveness (MINECO). NRN acknowledges support from Regione Campania L. 5/2002. The authors thank R. Peletier for the useful comments and suggestions to improve the paper and E. Toloba to have provided further information about the galaxy data set.

REFERENCES

Angus G. W., 2008, MNRAS, 387, 1481
Bartko H. et al., 2010, ApJ, 708, 834
Baugh C. M., Lacey C. G., Frenk C. S., Granato G. L., Silva L., Bressan A., Benson A. J., Cole S., 2005, MNRAS, 356, 1191
Begeman K. G., Broeils A. H., Sanders R. H., 1991, MNRAS, 249, 523
Bell E. F., McIntosh D. H., Katz N., Weinberg M. D., 2003, ApJS, 149, 289
Benson A. J., Cole S., Frenk C. S., Baugh C. M., Lacey C. G., 2000, MNRAS, 311, 793
Bertin G., Ciotti L., Del Principe M., 2002, A&A, 386, 149
Binggeli B., Sandage A., Tammann G. A., 1985, AJ, 90, 1681
Bullock J. S., Kolatt T. S., Sigad Y., Somerville R. S., Kravtsov A. V., Klypin A. A., Primack J. R., Dekel A., 2001, MNRAS, 321, 559
Buote D. A., Gastaldello F., Humphrey P. J., Zappacosta L., Bullock J. S., Brighenti F., Mathews W. G., 2007, ApJ, 664, 123
Capaccioli M., Caon N., D'Onofrio M., 1992, MNRAS, 259, 323
Cappellari M. et al., 2006, MNRAS, 366, 1126
Cappellari M. et al., 2012, Nature, 484, 485
Cappellari M. et al., 2013, MNRAS, 432, 1862
Cattaneo A., Dekel A., Faber S. M., Guiderdoni B., 2008, MNRAS, 389, 567
Chabrier G., 2003, PASP, 115, 763
Conroy C., van Dokkum P. G., 2012, ApJ, 760, 71
Conroy C., Wechsler R. H., 2009, ApJ, 696, 620
Dabringhausen J., Kroupa P., Pflamm-Altenburg J., Mieske S., 2012, ApJ, 747, 72
de Looze I. et al., 2010, A&A, 518, L54
Dekel A., Birnboim Y., 2006, MNRAS, 368, 2
Dutton A. A., Macciò A. V., 2014, MNRAS, 441, 3359
Dutton A. A., Macciò A. V., Mendel J. T., Simard L., 2013, MNRAS, 432, 2496
Famaey B., Binney J., 2005, MNRAS, 363, 603
Ferreras I., La Barbera F., de la Rosa I. G., Vazdekis A., de Carvalho R. R., Falcón-Barroso J., Ricciardelli E., 2013, MNRAS, 429, L15
Geha M., Guhathakurta P., van der Marel R. P., 2002, AJ, 124, 3073
Geha M. et al., 2013, ApJ, 771, 29
Gnedin O. Y., Kravtsov A. V., Klypin A. A., Nagai D., 2004, ApJ, 616, 16
Goudfrooij P., Kruijssen J. M. D., 2013, ApJ, 762, 107
Goudfrooij P., Kruijssen J. M. D., 2014, ApJ, 780, 43
Harding B., Tremblay C., Cousineau D., 2014, Quant. Methods Psychol., 10, 107
Hyde J. B., Bernardi M., 2009, MNRAS, 394, 1978
Janz J., Lisker T., 2009, ApJ, 696, L102
Janz J. et al., 2014, ApJ, 786, 105
Kormendy J., Fisher D. B., Cornell M. E., Bender R., 2009, ApJS, 182, 216
Kroupa P., 2001, MNRAS, 322, 231
Kuntschner H. et al., 2010, MNRAS, 408, 97
La Barbera F., de Carvalho R. R., Kohl-Moreira J. L., Gal R. R., Soares-Santos M., Capaccioli M., Santos R., Sant'anna N., 2008, PASP, 120, 681
La Barbera F., de Carvalho R. R., de La Rosa I. G., Lopes P. A. A., Kohl-Moreira J. L., Capelato H. V., 2010, MNRAS, 408, 1313
La Barbera F., Ferreras I., Vazdekis A., de la Rosa I. G., de Carvalho R. R., Trevisan M., Falcón-Barroso J., Ricciardelli E., 2013, MNRAS, 433, 3017
Leier D., Ferreras I., Saha P., 2012, MNRAS, 424, 104
Macciò A. V., Dutton A. A., van den Bosch F. C., 2008, MNRAS, 391, 1940
Marinoni C., Hudson M. J., 2002, ApJ, 569, 101
Matković A., Guzmán R., 2005, MNRAS, 362, 289
Milgrom M., 1983, ApJ, 270, 371
Moore B., Governato F., Quinn T., Stadel J., Lake G., 1998, ApJ, 499, L5
Moster B. P., Somerville R. S., Maulbetsch C., van den Bosch F. C., Macciò A. V., Naab T., Oser L., 2010, ApJ, 710, 903
Nagashima M., Lacey C. G., Baugh C. M., Frenk C. S., Cole S., 2005, MNRAS, 358, 1247
Napolitano N. R. et al., 2005, MNRAS, 357, 691
Napolitano N. R., Romanowsky A. J., Tortora C., 2010, MNRAS, 405, 2351
Navarro J. F., Frenk C. S., White S. D. M., 1996, ApJ, 462, 563
Navarro J. F., Frenk C. S., White S. D. M., 1997, ApJ, 490, 493
Paudel S., Lisker T., Kuntschner H., 2011, MNRAS, 413, 1764
Prantzos N., Charbonnel C., 2006, A&A, 458, 135
Recchi S., 2014, Adv. Astron., 2014, 4
Ryś A., van de Ven G., Falcón-Barroso J., 2014, MNRAS, 439, 284
Salpeter E. E., 1955, ApJ, 121, 161
Sanders R. H., McGaugh S. S., 2002, ARA&A, 40, 263

Shen S., Mo H. J., White S. D. M., Blanton M. R., Kauffmann G., Voges W., Brinkmann J., Csabai I., 2003, MNRAS, 343, 978
Shu Y. et al., 2015, ApJ, 803, 71
Smith R. J., 2014, MNRAS, 443, L69
Smith R. J., Lucey J. R., Conroy C., 2015, MNRAS, 449, 3441
Spiniello C., Trager S. C., Koopmans L. V. E., Chen Y. P., 2012, ApJ, 753, L32
Spiniello C., Trager S., Koopmans L. V. E., Conroy C., 2014, MNRAS, 438, 1483
Spolaor M., Kobayashi C., Forbes D. A., Couch W. J., Hau G. K. T., 2010, MNRAS, 408, 272
Swindle R., Gal R. R., La Barbera F., de Carvalho R. R., 2011, AJ, 142, 118
Thomas J. et al., 2011, MNRAS, 415, 545
Toloba E., Boselli A., Cenarro A. J., Peletier R. F., Gorgas J., Gil de Paz A., Muñoz-Mateos J. C., 2011, A&A, 526, A114
Toloba E., Boselli A., Peletier R. F., Falcón-Barroso J., van de Ven G., Gorgas J., 2012, A&A, 548, A78
Toloba E. et al., 2014, ApJS, 215, 17
Tortora C., Napolitano N. R., Romanowsky A. J., Capaccioli M., Covone G., 2009, MNRAS, 396, 1132
Tortora C., Napolitano N. R., Cardone V. F., Capaccioli M., Jetzer P., Molinaro R., 2010, MNRAS, 407, 144
Tortora C., Napolitano N. R., Romanowsky A. J., Jetzer P., Cardone V. F., Capaccioli M., 2011, MNRAS, 418, 1557
Tortora C., La Barbera F., Napolitano N. R., de Carvalho R. R., Romanowsky A. J., 2012, MNRAS, 425, 577
Tortora C., Romanowsky A. J., Napolitano N. R., 2013, ApJ, 765, 8
Tortora C., Romanowsky A. J., Cardone V. F., Napolitano N. R., Jetzer P., 2014a, MNRAS, 438, L46
Tortora C., La Barbera F., Napolitano N. R., Romanowsky A. J., Ferreras I., de Carvalho R. R., 2014b, MNRAS, 445, 115
Treu T., Auger M. W., Koopmans L. V. E., Gavazzi R., Marshall P. J., Bolton A. S., 2010, ApJ, 709, 1195
van den Bosch F. C. et al., 2007, MNRAS, 376, 841
Vazdekis A., Ricciardelli E., Cenarro A. J., Rivero-González J. G., Díaz-García L. A., Falcón-Barroso J., 2012, MNRAS, 3156
Wegner G. A., Corsini E. M., Thomas J., Saglia R. P., Bender R., Pu S. B., 2012, AJ, 144, 78
Weidner C., Ferreras I., Vazdekis A., La Barbera F., 2013, MNRAS, 435, 2274
Wolf J., Martinez G. D., Bullock J. S., Kaplinghat M., Geha M., Muñoz R. R., Simon J. D., Avedo F. F., 2010, MNRAS, 406, 1220
Woo J., Courteau S., Dekel A., 2008, MNRAS, 390, 1453

This paper has been typeset from a TEX/LATEX file prepared by the author.